Journal of King Saud University – Science 31 (2019) 1235–1244

Contents lists available at ScienceDirect

Journal of King Saud University – Science

journal homepage: www.sciencedirect.com

Azadirachta indica as a bio-material: Rapid synthesis of Cr_5O_{12} shell nanoparticles to study its photocatalytic and antimicrobial properties

Karthiga Rajendaran [a], Rajarajan Muthuramalangam [a,*], Suganthi Ayyadurai [b,*]

[a] Directorate of Distance Education, Madurai Kamaraj University, Palkalai Nagar, Madurai-625 021, Tamil Nadu, India
[b] PG & Research Department of Chemistry, Thiagarajar College, Madurai 625 009, Tamil Nadu, India

ARTICLE INFO

Article history:
Received 6 August 2018
Accepted 7 November 2018
Available online 8 November 2018

Keywords:
Cr_5O_{12}
Azadirachta indica
Photocatalysis
Methyl orange
Antimicrobial activity

ABSTRACT

A novel Cr_5O_{12} nanoparticle were prepared by reducing $K_2Cr_2O_7$ using *Azadirachta indica* plant extracts as a reducing agent. The synthesized nanoparticles shows orthorhombic phases with a band gap for 1.27 eV and it is further conformed by SEM. The average dimension of the nanoshell was about 56.99 nm. The FTIR spectrum explores the presence of the functional group of plant extract and Cr_5O_{12}. GC–MS of the aqueous extract shows the presence of many antioxidants in the leaf of *Azadirachta indica*. The photocatalytic performance was analyzed based on the degradation of Methyl Orange (MO) dye. The rate constant k of AzI-Cr_5O_{12} is found to be 3.93×10^{-2} s^{-1} and follows pseudo first-order kinetic at a catalyst dosage of 0.050 g/L with concentration of 20 μM of dye. Further, the antimicrobial activity of the nanoparticles was tested against *Staphylococcus aureus, Candida albicans* and *Enterobacter.*

1. Introduction

Nanoparticles having one or more dimensions in the order of 100 nm or less has noticeable attention and charming properties like optical, electronic, magnetic, etc., over their bulk counterparts (Daniel and Astruc, 2004; Kato, 2011). Size and shape of synthesized nanoparticles by chemical technique can be controlled and their defined morphologies are restored and improved in many catalytic applications (Li et al., 2004). Currently, sustainability drive that use of green chemistry to develop and/or protect our environment is becoming principal issues in many fields of research. Plants or plant extract is a new simple and environmentally friendly biosynthesis method (Kaviyarasu et al., 2017; Kaviyarasu et al., 2017). It is more beneficial over chemical and physical method beyond using pressure, temperature and toxic chemicals (Stern and Grasselli, 1997; Sundaram and Nagaraja, 2004; Pandey et al., 2006; Asif, 2012).

Chromic Oxide is a transition metal oxide with a variety of applications in many fields like the heterogeneous catalyst, coating material, wear resistance, advanced colorant, pigment and solar energy collector (Cui et al., 2015; Kim et al., 2004; Bobet et al., 2003; Zhang et al., 2013). Cr_2O_3 is a p – type semiconductor with a wide gap of 3.4 eV synthesized by simple (Khamlich et al., 2012; Jankovsky et al., 2015; Pei and Zhang, 2008; Puerari et al., 2016) functinalized by WO_3 nanorods (Choi et al., 2018), thermal decomposition (Gunnewiek et al., 2014) microwave refluxing and plasma (Su et al., 2014; Grzybowska et al., 1998) doped PVDF thin flims (Al-Hazmi et al., 2017) and coated with γ-Fe_2O_3 (Nadeema et al., 2018) have been employed. Green synthesis of Cr_2O_3 using plant such as Mukia Maderaspatna (Ananda and Gowda, 2013), Arachis Hypogaea (Ramesh et al., 2012) and synthesis of Cr_5O_{12} has not reported earlier.

The treatment of textile dye wastewaters in order to reduce visual color and dissolved organic contaminants to meet the increasing environmental demands have continued to attract the interest of research (Ramesh et al., 2012; Gupta et al., 2015; Gupta et al., 2013; Ahmaruzzaman and Gupta, 2011) Adsorption is widely used techniques for the separation and removal of pollutants from wastewaters (Mohammadi et al., 2011; Robati et al., 2016; Gupta et al., 2016; Asfaram et al., 2015). Photocatalytic oxidation using semiconductor is one of the advanced cost effective and green technology for the eradication of toxic organic and inorganic pollutants from textile dye wastewater (Reddy et al., 2018; Karthikeyan et al., 2012; Rajendran et al., 2016; Saravanan et al.,

* Corresponding authors.
E-mail addresses: rajarajanchem1962@gmail.com (R. Muthuramalangam), suganthitcarts@gmail.com (S. Ayyadurai).

Peer review under responsibility of King Saud University.

Production and hosting by Elsevier

https://doi.org/10.1016/j.jksus.2018.11.005
1018-3647/

2013; Saravanan et al., 2013; Saravanan et al., 2013; Saravanan et al., 2013; Saravanan et al., 2015; Magdalane et al., 2017; Magdalane et al., 2017; Biswas et al., 2002; Subapriya and Nagini, 2005).

A different section of the *Azadirachta indica* (Meliaceae family) has hold in universal medicine in the peculiar area around the nature (Uko and Kamalu, 2001; Angel Ezhilarasi et al., 2016). In particular, the leaf of neem is a "Storehouse" of organic compounds. There are ethnophormacological reports supporting their use against bacteria and worm infections by the oral use of their leave extracts. This effective pathogenic action is due to the existence of the alkaloids, flavonoids, glucoside, steroid, soluble carbohydrate, tannin, hydrogen cyanide and Azadirachtin (Matinise et al., 2017). In surface modification with plant extract the transition metal nanoparticles have various proven results that show cytotoxicity against microbes as is evident from the distortion of the morphology of the cells.

The phenolic compounds like flavonoids in the plant extracts are soluble in water, non toxic, bio-degradable and can function as both reducing agents for the synthesis of metal oxide (Raja et al., 2018; Angel Ezhilarasi et al., 2018; Valdez and Gomez, 2016; Karimiana and Pirib, 2013). On the surface of nanoparticles and this interaction could agglomerate more nanoparticles for making a bigger nanoparticle (Harborne et al., 1973). In addition, no reports on the synthesis of Cr_5O_{12} using aqueous neem extract have been published. The chemical constituent present in the aqueous extracts of neem leaves was analyzed by photochemical testing and Gas-chromatography-Mass spectrum (GC–MS) techniques. The photocatalytic performance of the Cr_5O_{12} nanoshell was measured related to the degradation of methyl orange. Further, the synthesized nanoshell was analyzed for cytotoxicity against antimicrobial like Candida albicans, Staphylococcus aureus, and Enterobacter as experimental pathogens which can be used for biomedical application.

2. Experiment

2.1. Materials and method

Analytical grade chemicals were purchased from 'MERCK chemicals' India. The young *Azadirachta indica* leaves were collected from C.P.A College, Bodinayakanur. Throughout the synthesis double distilled water was used. (i) *Azadirachta indica* plant leaves were used to make the aqueous extracts. Taxonomically authenticated healthy leaves were collected and about 25 g of leaves was thoroughly washed with distilled water, air desiccated, cut into fine pieces and boiled with 100 ml of distilled water in an Erlenmeyer flask for 10 min at 60 °C. The broth was filtered and stored at a temperature of 4 °C (Siddiqui and Ali, 1997). (ii) Typically 14.5 g of potassium dichromate was dissolved in 10 ml of plant extract and adjusted to 50 ml with distilled water. The plant extract was added to adjust the pH 8 and stirring is continued for 2 h. The synthesized AzI-Cr_5O_{12} nanoshells was washed and dried at room temperature and calcination is continued for 1 h in a muffle furnace at 500 °C (Buvaneswari et al., 2015).

2.2. Identification tests for active compounds

The aqueous extract of *Azadirachta indica* leaves monitored for various test for the phytochemical constituents by the following test (Iyengar, 1995).

S. No	PHYTOCHEMICALS	EXPERIMENT	INFERENCE
1	Alkaloids	Extract residue + 2% hydrochloric acid heated in a boiling-water bath.	Yellow precipitation
2	Carbohydrate	2 ml extract + 2 drops of alcoholic α-naphthol + 1mlconcentrated sulphuric acid	Violetring junction at the
3	Reducing sugar	0.5 ml extract + 1 ml water + 5 drops Fehling's solution	Brick red precipitate
4	Flavonoid	Extract + 1.5 ml of 50% methanol + metal magnesium and warmed, then 6 drops concentrated hydrochloric acid	Red colour solution
5	Glycoside	Glacial acetic acid + extract + ferric chloride + concentrated sulphuric acid	Reddish-brown colour at the junction
6	Tannins	1 ml of water + 0.5 ml of extract + 1 – drops of ferric chloride.	Formation of green or violet colour
7	Saponin	The extract was shaken for 15 min in a graduated cylinder with distilled water.	Formation of a layer of foam
8	Terpenoid steroid and	Extract + 0.5 ml of acetic anhydride + 0.5 ml of chloroform + concentrated sulphuric acid	Redvioletcolor (Trepenoid), bluish colour (steroids).
9	Protein	1 ml of 10% sodium hydroxide + heating + 0.7%coppersulphate solution	Violet or pink colour

2.3. Characterization

The phase composition and the crystallite size of Cr_5O_{12} were determined using an X- ray diffractometer (XRD; XPERT PRO X-RAY) with Cu Ka radiation at 25 °C and the structural assignments were made with reference to the JCPDS files. JSM 6701F—6701 microscope is used to analyze the surface morphology in both secondary and backscattered electron modes, in addition to the elemental analysis. JASCO V-550 double beam spectrophotometer was used to identify the optical properties of nanoshell with PMT detector. JASCO-FT-IR-460 plus was used for surface structure analysis of the nanoshell. EUTECH instrument was used for pH monitoring. Perkin-Elmer GC Clarus 500 system comprising an AOC-20 i auto-sampler was used for phytochemical analysis of the leaves.

2.4. Photocatalytic activity

300 ml aqueous solution of MO with a certain amount of photocatalyst was taken in the cylindrical glass vessel, which was surrounded by a circulating water jacket to cool the lamp. The air was bubbled continuously into the aliquot by an air pump in order to provide a constant source of dissolved oxygen. Before switching on irradiation, the suspension was stirred in the dark for 30 min to ensure that the adsorption – desorption equilibrium (Valdez and Gomez, 2016). 300 W Xe arc lamp with an ultraviolet ($\lambda < 400$ nm) cutoff filter was used as the visible-light irradiation source. During light irradiation, 5 ml aliquots were withdrawn at a regular time interval of 30 min. Then the samples were centrifuged and filtered through a millipore filter to remove the photocatalyst. The filtrate was analyzed by UV–Vis spectrophotometer at λ max = 465 nm and the photodegradation percentage were calculated by the expression given below:

$$\text{Photodegradation}(\%) = \frac{C_o - C}{C_o} \times 100 \quad (1)$$

where C_0 is the concentration of MO before irradiation and C is the concentration of MO after a certain irradiation time

2.5. Assay for antimicrobial activity of Cr_5O_{12} against microorganisms

The Cr_5O_{12} nanoparticles in sterilized distilled water were tested for their antibacterial activity by the agar diffusion method. Fungal strains (*Candida albicans*) and bacterial strains (*Staphylococcus aureus, Enterobacter)* were used to study the antimicrobial property (Saravanan et al., 2013). These bacillus were matured in nutrient agar media for 24 h anterior to the trial, were shown in agar plates by the pour plate technique. The five test organisms were swapped over the nutrient agar medium and the disks containing Cr_5O_{12} nanoparticles were kept over the medium using sterile forceps. The plates were nurtured at 37 °C for 24 h. The zone of restraint is deliberate in milimeter.

3. Result and discussion

3.1. Characterization

3.1.1. UV–Vis and UV–vis-DRS of Cr_5O_{12}

The UV–Visible spectroscopy is used to conform the reaction between metal ions and the leaf extracts for the formation of Cr_5O_{12} nanoshell (Fig. 1(a)). The peak at 325 nm is due to inter band transition of core electrons of chromium and chromium oxide. The light absorption ability of Cr_5O_{12} was studied by UV–Vis-DRS was shown Fig. 1(b). As seen in Fig. 1(c) the absorption edge of AzI-Cr_5O_{12} was highly shifted to the visible region. The band gap of semiconductors is correlated to its range of absorption wavelength, and the band gap decreases with increasing of absorption edge. The evaluation of band gaps can be done using Tauc approach (Karthiga et al., 2015).

$$\alpha = \frac{C\left(h\nu - E_g^{bulk}\right)^2}{h\nu} \quad (2)$$

where α is the absorption coefficient, $h\nu$ is the photon energy, E_g^{bulk} the optical band gap energy, h is the plank constant and c is the constant depending on the electron – hole mobility. A plot of $(\alpha h\nu)^{1/2}$

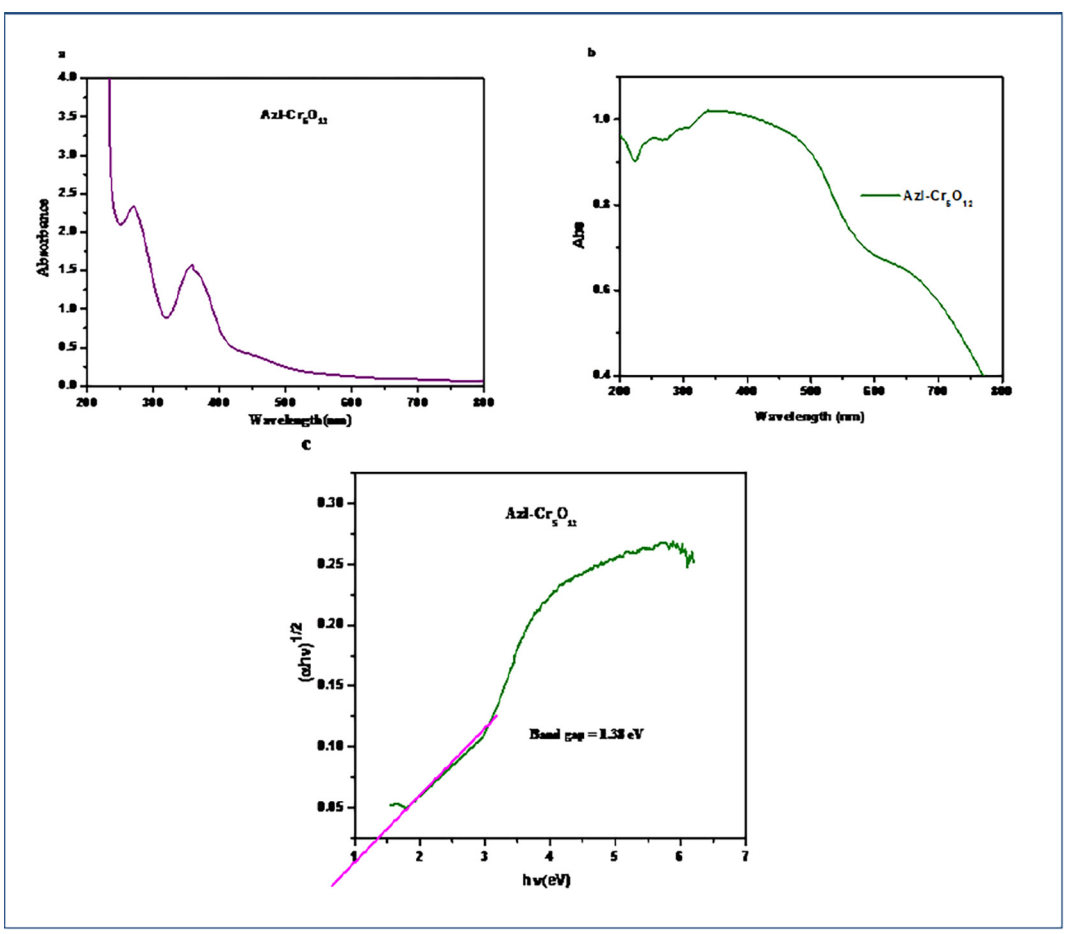

Fig. 1. (a). UV–Vis absorption spectrum of AzI-Cr_5O_{12} nanoparticles in aqueous solution, (b). UV–vis- DRS of AzI-Cr_5O_{12}, (c). Tauc plot of AzI-Cr_5O_{12}.

versus hν afforded band gap of both the samples. The band gap values of AzI-Cr_5O_{12} was found to be 1.35 eV while chromic oxide was found to be 3.4 ev prepared via chemical method (Karthiga et al., 2018). The light absorption efficiency significantly improved via surface modification using plant extract.

3.1.2. FTIR

The FTIR spectrum of the plant extract and plant extract (Fig. 2.) modified Cr_5O_{12} nanoparticles exhibited peaks at 3386 cm^{-1}, 1626 cm^{-1}, 1389 cm^{-1}, 1276 cm^{-1}, 1078 cm^{-1}, 760 cm^{-1} and 563 cm^{-1}. The band at 3386 cm^{-1} is assigned to the hydroxyl group of polyphenols. The characteristic peaks at 1626 cm^{-1} represented the carbonyl group (–C=O) of amide in proteins. The peaks at 1389 cm^{-1} and 1276 cm^{-1} may be assigned to the –N=O bending and inplane (–C–H) bending, respectively (Ikram and Inamul, 1984; Scarano et al., 1993). The absorption band at 1078 cm^{-1} is attributed to the –C–N stretching vibration of aliphatic amines. The characteristic peak at 760 cm^{-1} is designated to the –C–C–C– deformations of the phenyl ring. The peak at 947 cm^{-1} and 564 cm^{-1} indicates that Cr=O and Cr–O vibration of Cr_2O_3 nanoparticles in AzI- Cr_5O_{12} spectrum (Saleh and Gupta, 2011). From the examination terpenoids, flavonoids containing carboxyl group (capping agent) were found adsorbed on the surface of the nanoparticles. This also throws some light on the dual role of biological molecule in reducing metal ions and capping. Capping of nanoparticles by protein stabilizes Cr_5O_{12} nanoparticles and prevents agglomeration in the medium (Saleh and Gupta, 2012).

3.1.3. XRD

Fig. 3. shows the XRD pattern of AzI-Cr_5O_{12} nanoparticles. All the peaks can be indexed to the known orthorhombic structure of the Cr_5O_{12} (JCPDS No 73–1787). A series of characteristic peaks at 24.06° (0 2 1), 26.39° (3 1 1) and 39.00° (4 2 1) was observed. The high crystallinity AzI-Cr_5O_{12} was identified via strong intensity and narrow width diffraction peaks. In general, use of plant extract influence the polarity and coordinating ability can influence the morphology and crystallization behavior of the nanoshell and the reduction in microstrain are improved. The size of nanoparticles using XRD pattern has been estimated from scherrer equation and the average crystallite size for AzI-Cr_5O_{12} was determined as 56.99 nm (Vinoth et al., 2012; Ramadass and Subramanian, 2018).

$$D = \frac{K\lambda}{\beta\cos\theta} \quad (3)$$

where, β is the full width half maximum of the most intense 2θ peak, K is the shape factor (0.90). θ and λ are the incident angle and wavelength of X-rays respectively.

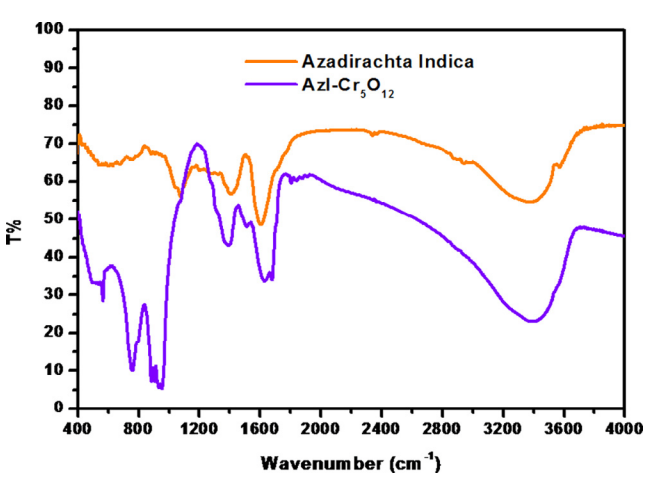

Fig. 2. FTIR spectra of AzI-Cr_5O_{12}.

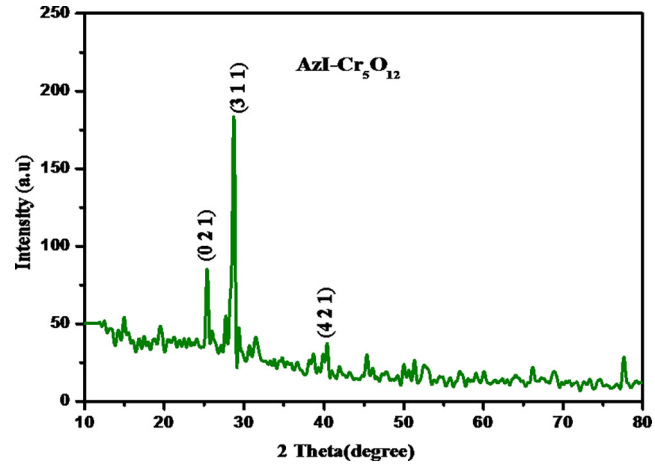

Fig. 3. XRD for AzI-Cr_5O_{12}.

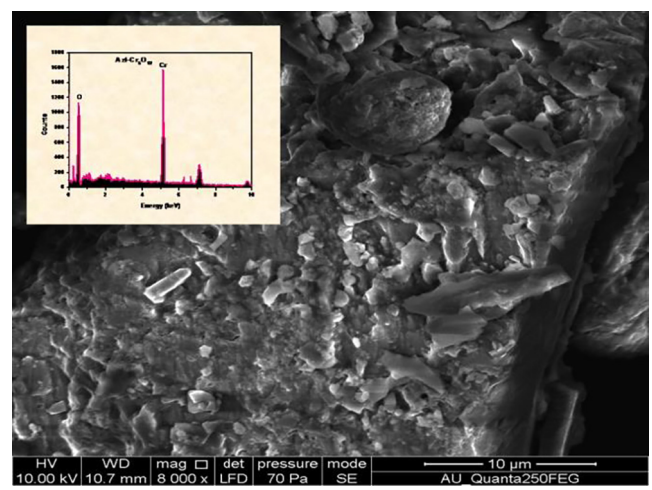

Fig. 4. (a). SEM image of AzI-Cr_5O_{12}, (Inset figure EDX spectrum of Cr_5O_{12}).

3.1.4. SEM and EDX

The morphology of AzI-Cr_5O_{12} is shown in the Fig. 4(a). The image reveals that the nanoparticles have shells and plate like structure. An EDX analysis was conducted on AzI- Cr_5O_{12} to determine the weight percentage of the AzI-Cr_5O_{12} and is displayed in inset figure and Table 1. It is found that the major elements of nanoshell are Cr and O clearly observed at their corresponding keV values without any impurity (Ramadass and Subramanian, 2018). AzI-Cr_5O_{12} was small in size, nearly spherical in shape and are agglomerated, due to the phytochemical present in the aqueous extract of *Azadirachta indica* and weak interparticle forces between the nanopartcles and secondary metabolites.

3.2. Qualitative determination of phytochemical in aqueous leaf extract

A various phytochemical that are present in the leaves of *Azadirachta indica* are responsible for the reduction and capping agent for the synthesis of nanoparticles. Qualitative test of phytochemical was shown in the Table 2. Aqueous extract of *Azadirachta indica* shows the presence of Alkaloids, Carbohydrate, Protein, Tannins, Phenolic compounds, Flavanoids and Triterpenoids and this were further conformed by GCMS. Table 2. Phytochemical study of aqueous *Azadirachta indica* leaves extract.

Table 1
EDX data of AzI-Cr_5O_{12}.

S. No	Element	Weight (%)	Atomic %	keV
1	Cr	57.61	73.31	5.131
2	O	42.39	30.94	0.510

Table 2
Qualitative test of phytochemical in aqueous extract.

S. No	Phytochemical constituent	Result
1	Alkaloids	+
2	Carbohydrate	+
3	Reducing Sugar	+
4	Flavanoids	+
5	Glycosides	–
6	Tannins and phenolic compounds	+
7	Triterpenoids	+
8	Protein	+

Each test in triploids, "+" presence, "–" Absence.

3.2.1. GC–MS

The aqueous extract of *Azadirachta indica* showed five major peaks in GC–MS chromatogram (Fig. 5) and the NIST library has been used for comparison of the mass spectra (Table 3) demonstrate the presence of 12 phytocomponents. From the results, it was observed that the presence of Phenol, 2-methoxy, 3-(3-propenyl)-, Hexadecane, Dibuthyl phthalate, 1-iodo-2-methyldecane, Eicosane, Docosane, Nonacosane, Phytol, Gamma-Sitosterol, Icosapentaenoic acid, Heptasiloxane, hexadecamethyl, Hexahydrofarnesyl acetone were the major components in the extract. Table 3 lists the phytochemicals that afford to the medicinal property of the *Azadirachta indica* leaves. Gamma-Sitosterol and Phytol (Vignesh et al., 2012) were known for its potential antioxidant, antibacterial, antifungal, anti arthritic and prophylactic activities. Hexadecane, Dibuthyl phthalate, 1-iodo-2-methyldecane, Eicosane, Docosane and Nonacosane has gained importance due to its antifungal and anticancer action, and also used as an insecticide. Phenol,2-methoxy, 3-(3-propenyl)- is reported to possess high level antimicrobial activity against fish pathogens (Bansal et al., 2009). These secondary metabolites present in the aqueous solution obtained from Azardirachta indica have a potential application in reduction of metal ions and act as a capping agent. Plant extracts act as secondary metabolites on the surface of nanoshells to increase the activity against pathogens to destroy the cell wall effectively.

3.3. Photocatalytic activity

The photocatalytic activity of AzI-Cr_5O_{12} was investigated in an aqueous solution of MO at 20 μM, at a catalyst concentration of 0.050 g/L and irradiation time of 90 min. The degradation of MO is negligible in the absence of photocatalyst due to chemical reaction rather than adsorption and the degradation follows pseudo first-order kinetic model (Maria Magdalane, 2017).

$$\ln(C/C_o) = kt \quad (4)$$

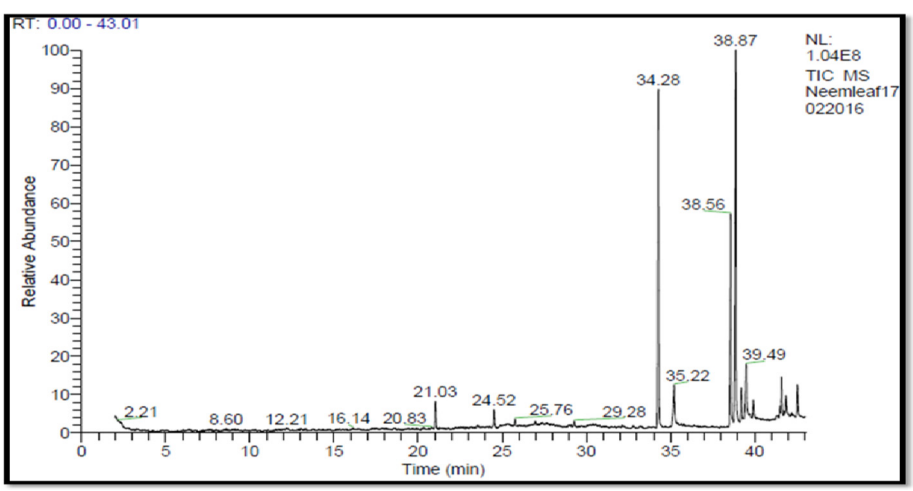

Fig. 5. GC–MS of aqueous neem extract.

Table 3
Chemical constituents and its Activity of some of the phytocomponents identified in the aqueous extracts of the Leaves of *Azadirachta indica* by GC–MS.

S. No	Retention Time	Name of the Compounds	Molecular Formula	Molecular Weight
1	12.21	Phenol, 2-methoxy, 3-(3-propenyl)-	$C_{10}H_{12}O_2$	164
2	16.14	Hexadecane	$C_{16}H_{34}$	226
3	20.83	Dibuthyl phthalate	$C_{16}H_{22}O_4$	278
4	21.03	1-iodo-2-methyldecane	$C_{11}H_{23}I$	296
5	21.03	Eicosane	$C_{20}H_{42}$	268
6	24.52	Docosane	$C_{22}H_{46}$	310
7	29.28	Nonacosane	$C_{29}H_{60}$	408
8	34.28	Phytol	$C_{20}H_{40}O$	296
9	34.28	Gamma-Sitosterol	$C_{29}H_{50}O$	414
10	38.56	Icosapentaenoic acid	$C_{20}H_{30}O_2$	302
11	38.87	Heptasiloxane, hexadecamethyl	$C_{16}H_{54}O_6Si_7$	533
12	39.49	Hexahydrofarnesyl acetone	$C_{18}H_{36}O$	268

where C_o was the initial concentration of MO at t = 0 min, C was the concentration of MO at the irradiation time 't' and k was the rate constant. The plot of –ln (C/C_o) versus irradiation time 't' was depicted in the Fig. 6. and a linear relationship was observed. At the experimental setting, it is identified that amount of MO (dye) after desorption–adsorption equilibrium is the initial amount C_O. According to the above kinetic model, the rate constant k of AzI-Cr_5O_{12} is found to be $3.93 \times 10^{-2}\ s^{-1}$. Since the nanoshells were prepared at a pH 8, the surface of adsorbent would be surrounded by the hydronium ions which enhance the dye interaction with binding sites of the biosorbent by greater attractive forces (Maria Magdalane et al., 2017). Therefore, the visible-light reactivity of Cr_5O_{12} is significantly enhanced by surface modification with plant extract.

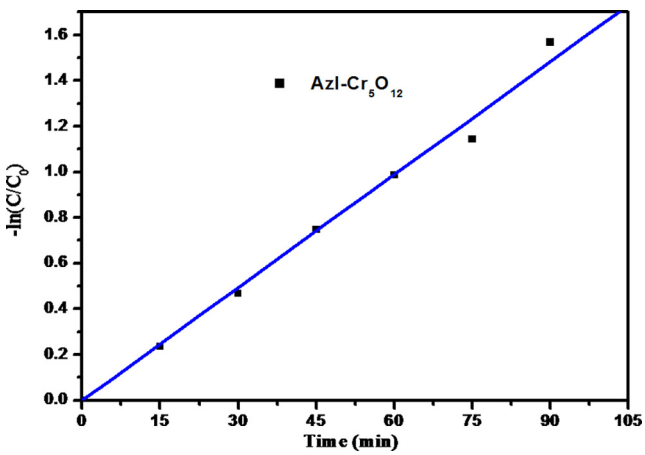

Fig. 6. Kinetic plot of $-\ln(C/C_o)$ versus irradiation time for the photodegradation of MO.

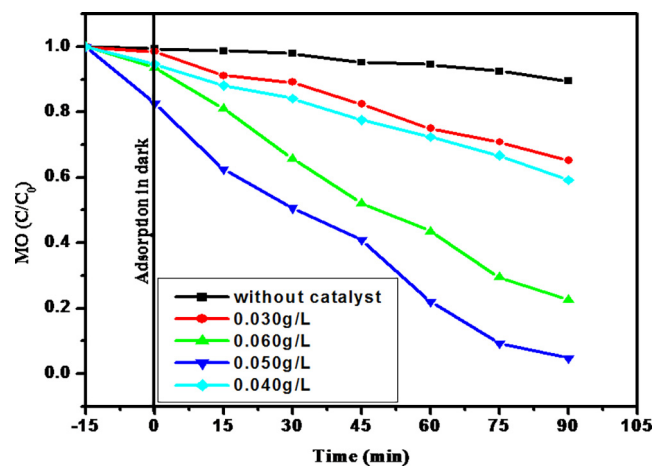

Fig. 8. Effect of AzI-Cr_5O_{12} dosage on the photodegradation of MO.

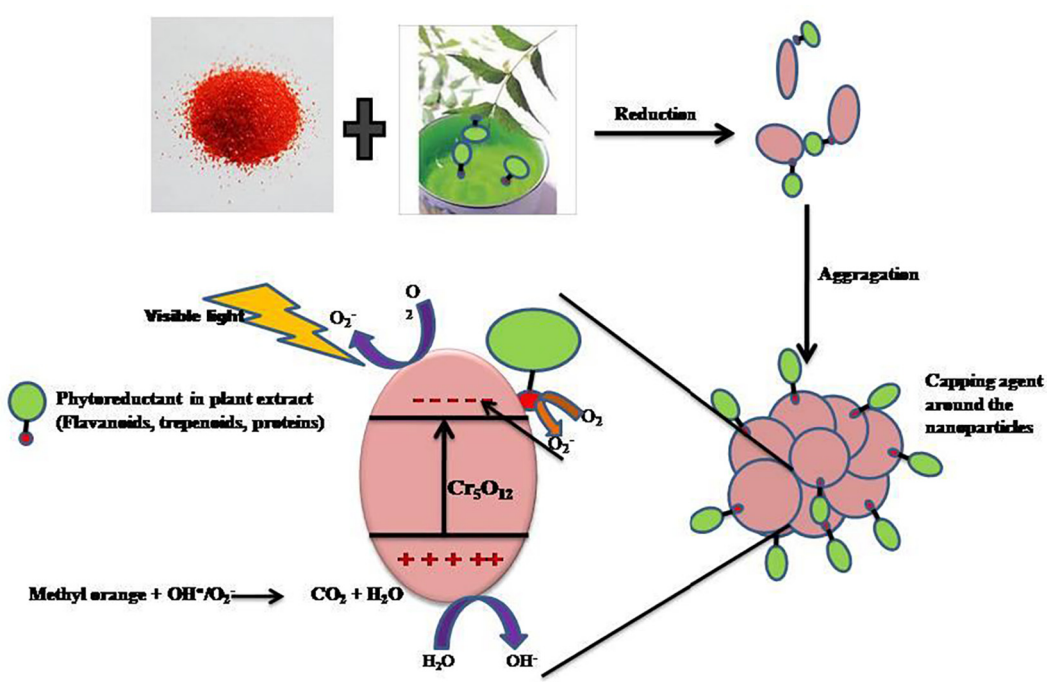

Fig. 7. Mechanism of Photocatalytic activity of AzI-Cr_5O_{12} under visible light irritation.

Table 4
Degradation efficiency of methyl orange solutions with other nanoparticles.

S. No	Nanoparticles	Light source	Dye Concentration	Percentage of degradation	References
1	V_2O_5 nanorods	Visible	5 μM	48(300 min)	(Liu et al., 2018)
2	AuNPs-TiO_2	Visible	10 μM	95(180 min)	(Ahluwalia et al., 2016)
3	Cu-ZnO nanorods	Solar	10 μM	95(120 min)	(Rabea et al., 2003)
5	TiO_2/HAP	UV	5 μM	92(150 min)	(Arunadevi et al., 2018)
6	Se-ZnS(green)	UV	20 μM	95(180 min)	(Angel Ezhilarasi et al., 2018)
7	AzI-Cr_5O_{12}	Visible	20 μM	95(90 min)	Present work

3.3.1. Mechanism

When the photocatalyst is irradiated by visible light, phytochemical present in the plant extract loaded on the surface of the Cr_5O_{12} can easily excited and create mobile electron which transfer electrons into surface adsorbed O_2 (Mobeen Amanulla et al., 2018; Reddy et al., 2018) resulting in generating more reactive oxygen species ($O_2^{\cdot-}$). Therefore the photogenerated electrons of phytochemical will be easily transferred to the conduction band of Cr_5O_{12} (wide band gap semiconductor) lead to the formation of new active sites, which enhance the electron-hole separation and facilitate the rapid transfer of electrons from the catalyst to molecular oxygen. This results in more charge carriers to form reactive species, which promote the degradation of MO (Jayaraj et al., 2018; Islam et al., 2018; Perillo, 2018) are shown in Fig. 7. The degradation efficiency of methyl orange solutions with other nanoparticles was compared at different reaction conditions were shown in Table 4. And the results show that Cr_5O_{12} by plant extracts exhibit superior degradation efficiency when compared to chemically and green synthesized method

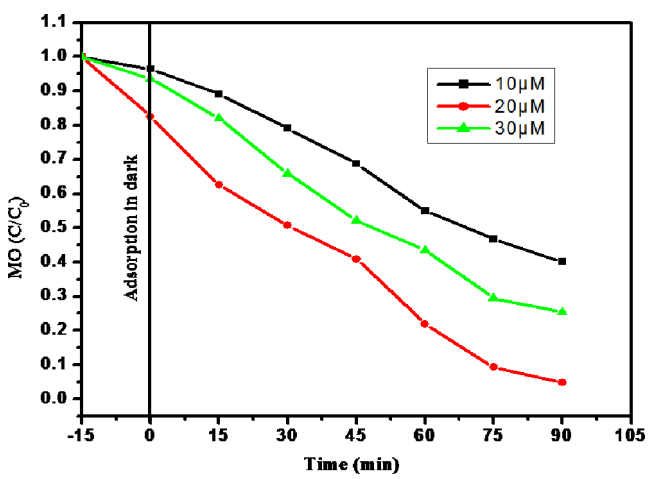

Fig. 9. Effect of initial MO concentration.

3.3.2. Effect of catalyst dosage

To evade the use of too much of a catalyst, it is comfortable to identify the optimum amount of catalyst for active degradation. A series of experiments was carried out by varying the dosage of catalyst from 0.030 to 0.060 g/L with a dye concentration of 20 μM and irradiation time of 90 min. The degradation efficiency of MO for various photocatalyst loadings is illustrated in Fig. 8. The results show that an increase in the catalyst loading from 0.030 to 0.050 g/L boost the dye degradation strongly from about 59% to 95%, due to the increases of mobile sites on the surface of the catalyst (Karthiga, 2015). Beyond 0.050 g/L of catalyst resulted in a decline in dye degradation. This abnormality is due to the interference and arrest of light penetration caused by the enormous amount of the catalyst. Particle aggregation is indicative at higher concentrations and reduces the active sites on the catalyst surface.

3.3.3. Effect of initial concentration of MO

MO varied from 10 to 30 μM to study the initial dye concentration (Fig. 9). The photodegradation of MO increases with increase of MO (10–20 μM) and then decreases with further increase of concentration (20–30 μM). The photodegradation performance was contrariwisely changed by the concentration of dye. The decrease in degradation with an increase in dye concentration was ascribed to the equilibrium adsorption of dye on the catalyst surface which results in the decrease of number of active sites. This phenomenon results in the formation of hydroxyl radicals, considered as a primary oxidizing agent of the dye (Saravanan et al., 2015).

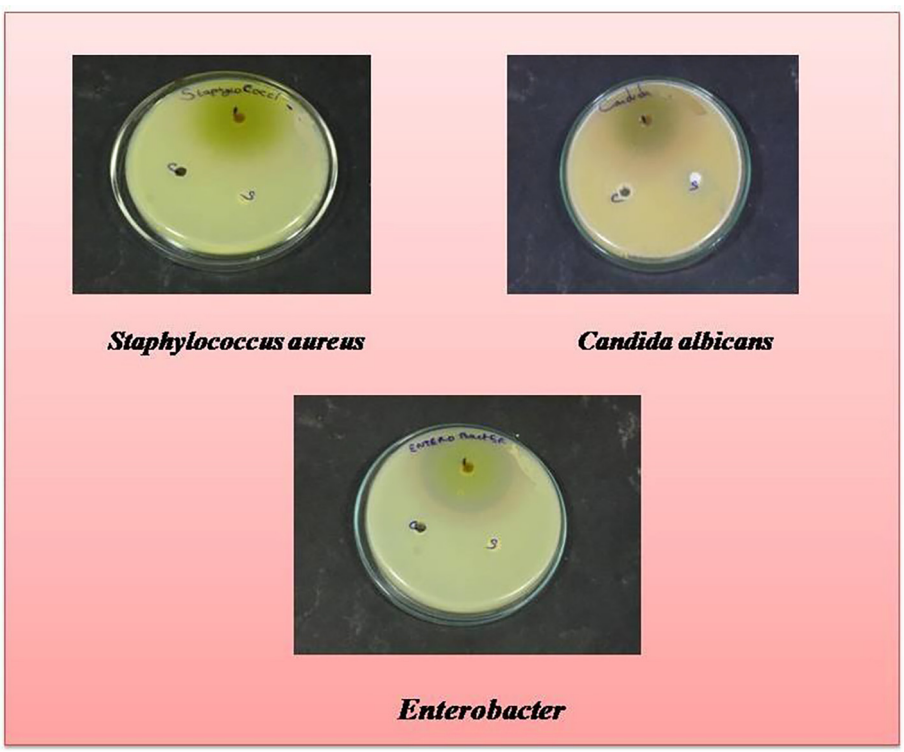

Fig. 10. Photograph of antimicrobial activity of AzI-Cr_5O_{12}.

Table 5
Antimicrobial activities of AzI-Cr_5O_{12}.

Type of Pathogens	Name of organism	Zone of inhibition in mm		
		Control (c) (Ketokonazole)	Standard (s) (Amikacin)	AzI- Cr_5O_{12}(1)
Gram +ve Bacteria	*Staphylococcus aureus*	18	R	40
Gram −ve Bacteria	*Enterobacter*	17	R	35
Fungal Species	*Candida albicans*	25	R	25

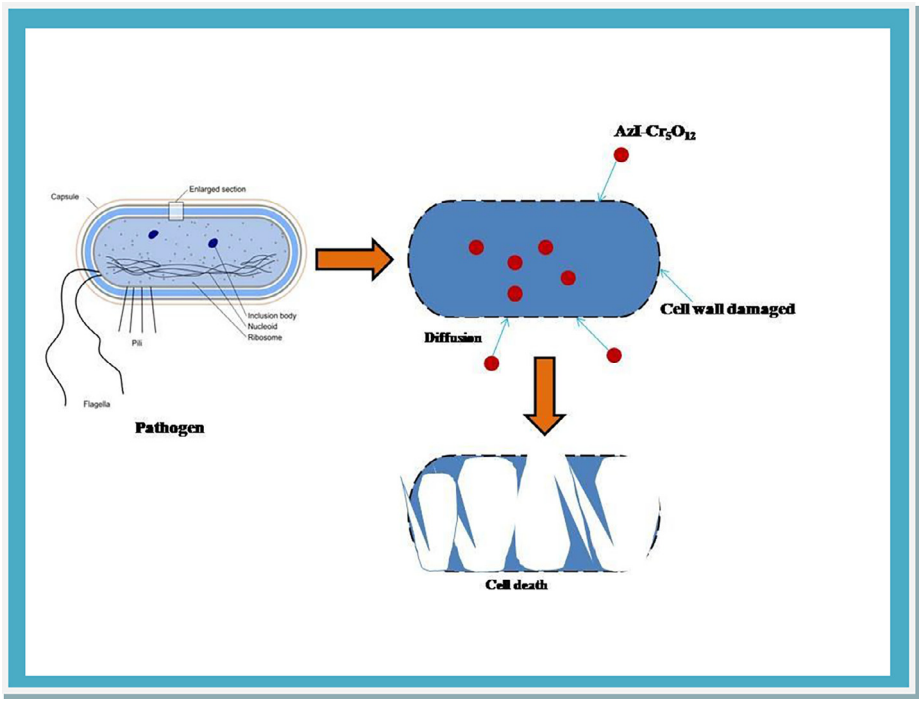

Fig. 11. Mechanism of Antimicrobial activity of AzI-Cr_5O_{12}.

3.4. Antimicrobial activity of Cr_5O_{12}

Fungal strains (*Candida albicans*) and bacterial strains (*Staphylococcus aureus and Enterobacter)* was analyzed using AzI-Cr_5O_{12} are shown in Fig. 10 and Table 5. represent the antimicrobial activity of AzI-Cr_5O_{12} for various microbes in a well diffusion assay. Amikacin was used as a reference drug and Ketokonazole as a control. The result revealed that AzI- Cr_5O_{12} shows excellent antimicrobial activity against a range of bacteria and fungi. A larger zone of inhibition was observed to AzI-Cr_5O_{12}, whereas smaller zone of inhibition for resistant strains. According to the zone of inhibition *Staphylococcus aureus* and *Enterobacter* (bacterial strain) exhibited the highest sensitivity toward Cr_5O_{12}. While *Candida albicans* (fungal strains) show the least sensitivity among the tested microbes. The microbial performance of AzI-Cr_5O_{12} depends on its degree of polymerization, molecular weight, nutrient composition, host, natural nutrient constituency, solvent, microorganism, physicochemical effect, and pH (Ezhilarasi et al., 2016; Mobeen Amanulla et al., 2018) was shown in Fig. 11.

4. Conclusion

AzI-Cr_5O_{12} nanoparticles have been successfully synthesized by simple co- precipitation method. Cr_5O_{12} nanoparticles were characterized by FT-IR, XRD, SEM and EDX techniques. The photocatalyst AzI-Cr_5O_{12} is successfully applied for the degradation of MO under visible light irradiation. The enhanced photocatalytic activity of AzI-Cr_5O_{12} is due to the suppression of electron-hole recombination by leaf extract in Cr_5O_{12}. The reaction conditions are optimized and maximum photodegradation is achieved within 90 min with an AzI-Cr_5O_{12} dosage of 0.050 g/L and MO concentration of 20 μM. A highest zone of inhibition was observed for *Staphylococcus aureus* and *Enterobacter* of about 40 and 35 mm respectively compared to other microorganisms.

References

Ahluwalia, S., Tejo Prakash, N., Prakash, R., Pal, B., 2016. Improved degradation of methyl orange dye using bio-co-catalyst Se nanoparticles impregnated ZnS photocatalyst under UV irradiation. Chem. Eng. J. 306, 1041–1048.
Ahmaruzzaman, M., Gupta, V.K., 2011. Rice husk and its ash as low-cost adsorbents in water and wastewater treatment. Ind. Eng. Chem. Res. 50, 13589–13613.
Al-Hazmi, F.S., de Leeuw, D.M., Al-Ghamdi, A.A., Shokr, F.S., 2017. Evaluation of the spectroscopic ellipsometry and dielectric properties of Cr_2O_3 nanoparticles doped PVDF thin films for future application of organic ferroelectric junctions. Optik 138, 207–213.
Ananda, R.S., Gowda, N., 2013. Synthesis of chromium(III) oxide nanoparticles by electrochemical method and mukia maderaspatana plant extract, characterization, $KMnO_4$ decomposition and antibacterial study. Mod. Res. Catal. 2 (4), 127–135.
Angel Ezhilarasi, A., Judith Vijaya, J., Kaviyarasu, K., Maaza, M., Ayeshamariam, A., Kennedy, J., 2016. Green synthesis of NiO nanoparticles using *Moringa oleifera* extract and their biomedical applications: cytotoxicity effect of nanoparticles against HT-29 cancer cells. J. Photochem. Photobiol. B: Biol. 164, 352–360.
Angel Ezhilarasi, A., Judith Vijaya, J., Kaviyarasu, K., John Kennedy, L., Jothi Ramalingam, R., Al-Lohedan, Hamad A., 2018. Green synthesis of NiO nanoparticles using *Aegle marmelos* leaf extract for the evaluation of in-vitro cytotoxicity, antibacterial and photocatalytic properties. J. Photochem. Photobiol. B: Biol. 180, 39–50.
Angel Ezhilarasi, A., Judith Vijaya, J., Kaviyarasu, K., John Kennedy, L., Jothiramalingam, R., Al-Lohedan, Hamad A., 2018. Green synthesis of NiO nanoparticles using Aegle marmelos leaf extract for the evaluation of in-vitro

cytotoxicity, antibacterial and photocatalytic properties. J. Photochem. Photobiol. B: Biol. 180, 39–50.
Arunadevi, R., Kavitha, B., Rajarajan, M., Suganthi, A., Jeyamurugan, A., 2018. Investigation of the drastic improvement of photocatalytic degradation of Congo red by monoclinic Cd, Ba-CuO nanoparticles and its antimicrobial activities. Surf. Interfaces 10, 32–44.
Asfaram, A., Ghaedi, M., Agarwal, S., Tyagi, I., Gupta, V.K., 2015. Removal of basic dye Auramine-O by ZnS: Cu nanoparticles loaded on activated carbon Optimization of parameters using response surface methodology with central composite design. RSC Adv. 5 (24), 18438–18450.
Asif, M., 2012. Antimicrobial potential of Azadirachta indica against pathogenic bacteria and fungi. J. Pharm. Phytochem. 4, 78.
Bansal, M., Garg, U., Singh, D., Garg, V.K., 2009. Removal of Cr (VI) from aqueous solutions using preconsumer processing agricultural waste: a case study of rice husk. J. Hazard. Mater. 162 (2009), 312–320.
Biswas, K., Chattopadhyay, I., Banerjee, R.K., Bandyopadhyay, U., 2002. Biological activities and medicinal properties of neem (Azadirachta indica). Curr. Sci. 82, 1336–1345.
Bobet, J.L., Desmoulins-Krawiec, S., Ficansell, E.G., Chevalier, B., 2003. Addition of nanosized Cr_2O_3 to magnesium for improvement of the hydrogen sorption properties. J. Alloys Compd. 351, 217–221.
Buvaneswari, K., Karthiga, R., Kavitha, B., Rajarajan, M., Suganthi, A., 2015. Effect of $FeWO_4$ doping on the photocatalytic activity of ZnO under visible light irradiation. Appl. Surf. Sci. 356, 333–340.
Choi, S., Bonyani, M., Sun, G.J., Lee, J.K., Hyun, S.K., Lee, C., 2018. Cr_2O_3 nanoparticle functionalized WO_3 nanorods for ethanol gas sensors. Appl. Surf. Sci. 432, 241–249.
Cui, C.Y., Xia, C.D., Cui, X.G., Zhou, J.Z., Ren, X.D., Wang, Y.M., 2015. Novel morphologies and growth mechanism of Cr_2O_3 oxide formed on stainless steel surface via Nd: YAG pulsed laser oxidation. J. Alloys Compd. 635, 101–106.
Daniel, M.C., Astruc, D., 2004. Gold nanoparticles: assembly, supramolecular chemistry, quantum-size-related properties, and applications toward biology, catalysis, and nanotechnology. Chem. Rev. 104, 293–346.
Ezhilarasi, A., Judith Vijaya, J., Kaviyarasu, K., Maaza, M., Ayeshamariam, A., John Kennedy, L., 2016. Green synthesis of NiO nanoparticles using Moringa oleifera extract and their biomedical applications: cytotoxicity effect of nanoparticles against HT-29 cancer cells. J. Photochem. Photobiol. B: Biol. 164, 352–360.
Grzybowska, B., Sloczynski, J., Grabowski, R., Wcislo, K., Kozlowska, A., Stoch, J., Zielinski, J., 1998. Chromium oxide/alumina catalysts in oxidative dehydrogenation of isobutane. J. Catal. 178 (2), 687–700.
Gunnewiek, R.F.K., Mendes, C.F., Kiminami, R.H.G.A., 2014. Synthesis of Cr_2O_3 nanoparticles via thermal decomposition of polyacrylate/chromium complex. Mater. Lett. 129, 54–56.
Gupta, V.K., Kumar, R., Nayak, A., Saleh, T.A., Barakart, M.A., 2013. Adsorptive removal of dyes from aqueous solution onto carbon nanotubes: a review. Adv. Colloid Interface Sci. 193–194, 24–34.
Gupta, V.K., Nayak, A., Agarwal, S., 2015. Bioadsorbents for remediation of heavy metals: current status and their future prospects. Environ. Eng. Res. 20 (1), 1–18.
Gupta, V.K., Nayak, A., Agarwal, S., Tyagi, I., 2016. Potential of activated carbon from Waste Rubber Tire for the adsorption of phenolics: effect of pre-treatment conditions. J. Colloid Interface Sci. 417, 420–430.
Harborne, J.B., 1973. In: Phytochemical Methods. 2nd ed. Chapman and Hall Ltd, London, pp. 49–188.
Ikram, M., Inamul, H., 1984. Screening of medicinal plants for antimicrobial activity. Part I, Fitoterapia 55, 231–235.
Maria Magdalane, C., Kaviyarasu, K., Judith Vijaya, J., Jayakumar, C., Maaza, M., 2017. Photocatalytic degradation effect of malachite green and catalytic hydrogenation by UV–illuminated CeO_2/CdO multilayered nanoplatelet arrays: investigation of antifungal and antimicrobial activities. J. Photochem. Photobiol. B: Biol. 169, 110–123.
Islam, Md.T., Jing, H., Yang, T., Zubia, E., Goos, A.G., Bernal, R.A., Botez, C.E., Narayan, M., Chan, C.K., Noveron, J.C., 2018. Fullerene stabilized gold nanoparticle supported on titanium dioxide for enhanced photocatalytic degradation of methyl orange and catalytic reduction of 4-nitrophenol. J. Environ. Chem. Eng. 6 (4), 3827–3836.
Iyengar, M.A., 1995. Study of Crude Drugs. Manipal Power Press, Manipal, India, p. 2.
Jankovsky, O., Sedmidubsky, D., Sofer, Z., Luxa, J., Bartunek, V., 2015. Simple synthesis of Cr_2O_3 nanoparticles with a tunable particle size. Ceram. Int. 41 (3), 4644–4650.
Jayaraj, S.K., Sadishkumar, V., Arun, T., Thangadurai, P., 2018. Enhanced photocatalytic activity of V_2O_5 nanorods for the photodegradation of organic dyes: a detailed understanding of the mechanism and their antibacterial activity. Mater. Sci. Semicond. Process. 85, 122–133.
Karimiana, R., Pirib, F., 2013. Synthesis and investigation the catalytic behavior of Cr_2O_3. J. Nanostruct. 3, 87–92.
Karthiga, R., Kavitha, B., Rajarajan, M., Suganthi, A., 2015. Photocatalytic and antimicrobial activity of $NiWO_4$ nanoparticles stabilized by the plant extract. Mater. Sci. Semicond. Process. 40, 123–129.
Karthiga, R., Kavitha, B., Rajarajan, M., Suganthi, A., 2018. Synthesis of MoO_3 microrods via phytoconsituents of Azadirachta indica leaf to study the cationic dye degradation and antimicrobial properties. J. Alloys Compound. 753, 300–307.
Karthiga, R., Sudha, A., 2015. Green synthesis of ZnO nanoparticles using sollanam santhocarbom to study its solar photocatalytic activity. IJSR 6 (6), 2370–2376.
Karthikeyan, S., Gupta, V.K., Boopathy, R., Titus, A., Sekaran, G., 2012. A new approach for the degradation of high concentration of aromatic amine by heterocatalytic Fenton oxidation: kinetic and spectroscopic studies. J. Mol. Liq. 173, 153–163.
Kato, H., 2011. *In vitro* assays: tracking nanoparticles inside cells. Nat. Nanotechnol. 6, 139–140.
Kaviyarasu, K., Geetha, N., Sivaranjani, S., Ayeshamariam, A., Kennedy, J., Ladchumananandasiivam, R., Umbelino Gomes, U., Maaza, M., 2017. In vitro cytotoxicity effect and antibacterial performance of human lung epithelial cells A549 activity of Zinc oxide doped TiO_2 nanocrystals: investigation of bio-medical application by chemical method. Mater. Sci. Eng. C 74, 325–333.
Kaviyarasu, K., Kanimozhi, K., Matinise, N., Maria Magdalane, C., Mola, Genene T., Kennedy, J., Maaza, M., 2017. Antiproliferative effects on human lung cell lines A549 activity of cadmium selenide nanoparticles extracted from cytotoxic effects: investigation of bio-electronic application. Mater. Sci. Eng. C 76, 1012–1025.
Khamlich, S., Nemraoui, O., Mongwaketsi, N., McCrindle, R., Cingo, N., Maaza, M., 2012. Black Cr/α-Cr_2O_3 nanoparticles based solar absorbers. Phys. B: Condens. Mater. 407 (10), 1509–1512.
Kim, D.W., Shin, S.L.I., Lee, J.D., Oh, S.G., 2004. Preparation of chromia nanoparticles by precipitation–gelation reaction. Mater. Lett. 58, 1894–1898.
Li, Y., White, T.J., Lim, S.H., 2004. Low-temperature synthesis and microstructural control of titania nano-particles. J. Solid State Chem. 177, 1372–1381.
Liu, W., Qian, G., Liu, L., Fan, X., Cai, X., Feng, J., Gao, M., 2018. The growth mechanism of titania/hydroxyapatite and its application in the photodegradation of methyl orange dye under UV irradiation. Results Phys. 11, 112–117.
Magdalane, C.M., Kaviyarasu, K., Judith Vijaya, J., Siddhardha, B., Jeyaraj, B., 2017. Facile synthesis of heterostructured cerium oxide/yttrium oxide nanocomposite in UV light induced photocatalytic degradation and catalytic reduction: synergistic effect of antimicrobial studies. J. Photochem. Photobiol. B: Biol. 173, 23–34.
Magdalane, C.M., Kaviyarasu, K., Judith Vijaya, J., Siddhardha, B., Jeyaraj, B., Kennedy, J., Maaza, M., 2017. Evaluation on the heterostructured CeO_2/Y_2O_3 binary metal oxide nanocomposites for UV/Vis light induced photocatalytic degradation of Rhodamine – B dye for textile engineering application. J. Alloys Compound. 727, 1324–1337.
Maria Magdalane, C., Kaviyarasu, K., Judith Vijaya, J., Siddhardha, B., Jeyaraj, B., Kennedy, J., Maaza, M., 2017. Evaluation on the heterostructured CeO_2/Y_2O_3 binary metal oxide nanocomposites for UV/Vis light induced photocatalytic degradation of Rhodamine – B dye for textile engineering application. J. Alloys Compound. 727, 1324–1337.
Matinise, N., Fuku, X.G., Kaviyarasu, K., Mayedwa, N., Maaza, M., 2017. ZnO nanoparticles via Moringa *oleifera* green synthesis: physical properties & mechanism of formation. Appl. Surf. Sci. 406, 339–347.
Mobeen Amanulla, A., Jasmine Shahina, S.K., Sundaram, R., Maria Magdalane, C., Kaviyarasu, K., Douglas Letsholathebe, S.B., Mohamed, J., Kennedy, M. Maaza, 2018. Antibacterial, magnetic, optical and humidity sensor studies of β-$CoMoO_4$ - Co_3O_4 nanocomposites and its synthesis and characterization. J. Photochem. Photobiol. B: Biol. 180, 39–50.
Mobeen Amanulla, A., Jasmine Shahina, S.K., Sundaram, R., Maria Magdalane, C., Kaviyarasu, K., Douglas Letsholathebe, S.B., Mohamed, J., Kennedy, M. Maaza, 2018. Antibacterial, magnetic optical and humidity sensor studies of β-$CoMoO_4$ - Co_3O_4 nanocomposites and its synthesis and characterization. J. Photochem. Photobiol. B: Biol. 183, 233–241.
Mohammadi, N., Khani, H., Gupta, V.K., Amereh, E., Agarwal, S., 2011. Adsorption process of methyl orange dye onto mesoporous carbon material–kinetic and thermodynamic studies. J. Colloid Interface Sci. 362, 457–462.
Nadeema, K., Kamrana, M., Javeda, A., Zeba, F., Hussaina, S.S., Mumtaza, M., Krennb, H., Szaboc, D.V., Brossmanne, U., 2018. Xiaoke Mu, Role of surface spins on magnetization of Cr_2O_3 coated γ-Fe_2O_3 nanoparticles. Solid State Sci. 83, 43–48.
Pandey, P.S., Bhave, N.S., Kharat, R.B., 2006. Structural, optical, electrical and photovoltaic electrochemical characterization of spray deposited $NiWO_4$ thin films. Electrochim. Acta 51, 4659–4664.
Pei, Z., Zhang, Y., 2008. A novel method to prepare Cr_2O_3 nanoparticles. Mater. Lett. 62, 504–506.
Perillo, P.M., Atia, M.N., 2018. Solar-assisted photodegradation of Methyl Orange using Cu-doped ZnO nanorods. Mater. Today Commun. https://doi.org/10.1016/j.mtcomm.2018.09.010.
Puerari, R.C., daCosta, C.H., Vicentini, D.S., Fuzinatto, C.F., Melegari, S.P., Schmidt, E. C., Bouzon, Z.L., Matias, W.G., 2016. Synthesis characterization and toxicological evaluation of Cr_2O_3 nanoparticles using Daphnia magna and Aliivibrio fischeri. Ecotoxicol. Environ. Safety 128, 36–43.
Rabea, E.I., Badawy, M.E., Stevens, C.V., Smagghe, G., Steurbaut, W., 2003. Chitosan as antimicrobial agent: applications and mode of action. Biomacromolecules 4 (6), 1457–1465.
Raja, A., Ashokkumar, S., Pavithra Marthandam, R., Jayachandiran, J., Kathiwada, Chandra Prasad, Kaviyarasu, K., Ganapathi Raman, R., Swaminathan, M., 2018. Eco-friendly preparation of zinc oxide nanoparticles using Tabernaemontana divaricata and its photocatalytic and antimicrobial activity. J. Photochem. Photobiol. B: Biol. 181, 53–58.
Rajendran, S., Khan, M.M., Gracia, F., Qin, J., Gupta, V.K., Arumainathan, S., 2016. Ce^{3+}-ion-induced visible-light photocatalytic degradation and electrochemical activity of ZnO/CeO_2 nanocomposite. Sci. Rep. 6, 31641–31652.
Ramadass, N., Subramanian, N., 2018. Study of phytochemical screening of neem (*Azadirachta indica*). Int. J. Zool. Stud. 3 (1), 209–212.

Ramesh, C., Mohan Kumar, K., Senthil, M., Ragunathan, V., 2012. Antibacterial activity of Cr_2O_3 nanoparticles against E. coli; reduction of chromate ions by Arachis hypogaea leaves. Achiev. Appl. Sci. Res. 4 (4), 1894–1900.
Reddy, Y.S., Magdalane, C.M., Kaviyarasu, K., Tessema, A.G., Kennedy, M.J., Maaza, M., 2018. Equilibrium and kinetic studies of the adsorption of acid blue 9 and Safranin O fromaqueous solutions by MgO decked FLG coated Fuller's earth. J. Phys. Chem. Solids 123, 43–51.
Reddy, S., Maria Magdalane, C., Kaviyarasu, K., Genene, A., Mola, T., Kennedy, J., Maaza, M., 2018. Equilibrium and kinetic studies of the adsorption of acid blue 9 and Safranin O from aqueous solutions by MgO decked FLG coated Fuller's earth. J. Phys. Chem. Solids 123, 43–51.
Robati, D., Mirza, B., Rajabi, M., Moradi, O., Tyagi, I., Agarwal, S., Gupta, V.K., 2016. Removal of hazardous Dyes-BR 12 and methyl orange using graphene oxide as an adsorbent from aqueous phase. Chem. Eng J. 284, 687–697.
Saleh, T.A., Gupta, V.K., 2011. Functionalization of tungsten oxide into MWCNT and its application for sunlight-induced degradation of rhodamine B. J. Colloid Interface Sci. 362, 337–344.
Saleh, T.A., Gupta, V.K., 2012. Synthesis and characterization of alumina nanoparticles polyamide membrane with enhanced flux rejection performance. Sep. Purif. Technol. 89, 245–251.
Saravanan, R., Gupta, V.K., Prakash, T., Narayanan, V., Stephen, A., 2013. Synthesis, characterization and photocatalytic activity of novel Hg doped ZnO nanorods prepared by thermal decomposition method. J. Mol. Liq. 178, 88–93.
Saravanan, R., Karthikeyan, N., Gupta, V.K., Thirumal, E., Thangadurai, P., Narayanan, V., Stephen, A., 2013. ZnO/Ag nanocomposite: an efficient catalyst for degradation studies of textile effluents under visible light. Mater. Sci. Eng. C 33, 2235–2244.
Saravanan, R., Joicy, S., Gupta, V.K., Narayanan, V., Stephen, A., 2013. Visible light induced degradation of methylene blue using CeO_2/V_2O_5 and CeO_2/CuO catalysts. Mater. Sci. Eng.C 33, 4725–4731.
Saravanan, R., Thirumal, E., Gupta, V.K., Narayanan, V., Stephen, A., 2013. The photocatalytic activity of ZnO prepared by simple thermal decomposition method at various temperatures. J. Mol. Liq. 177, 394–401.
Saravanan, R., Karthikeyan, S., Gupta, V.K., Sekaran, G., Narayanan, V., Stephen, A., 2013. Enhanced photocatalytic activity of ZnO/CuO nanocomposite for the degradation of textile dye on visible light illumination. Mater. Sci. Eng. C 33, 91–98.
Saravanan, R., Mansoob Khan, M., Gupta, V.K., Mosquera, E., Gracia, F., Narayanan, V., Stephen, A., 2015. $ZnO/Ag/Mn_2O_3$ nanocomposite for visible light-induced industrial textile effluent degradation, uric acid and ascorbic acid sensing and antimicrobial activities. RSC Adv. 5, 34645–34651.
Saravanan, R., Mansoob Khan, M., Gupta, V.K., Mosquera, E., Gracia, F., Narayanan, V., Stephen, A., 2015. ZnO/Ag/CdO nanocomposite for visible light-induced photocatalytic degradation of industrial textile effluents. J. Colloid Interface Sci. 452, 126–133.
Scarano, D., Zecchina, A., Bordiga, S., Ricchiardi, G., Spoto, G., 1993. Interaction of CO with α-Cr_2O_3 surface: a FTIR and HRTEM study. Chem. Phys. 177 (2), 547–560.
Siddiqui, A.A., Ali, M., 1997. Practical Pharmaceutical Chemistry. CBS Publishers and Distributors, New Delhi, pp. 126–131.
Stern, D.L., Grasselli, R.K., 1997. Propane oxydehydrogenation over metal tungstates. J. Catal. 167, 570–572.
Su, J., Xue, H., Gu, M., Xia, H., Pan, F., 2014. Synthesis of spherical Cr_2O_3 nanoparticles by a microwave refluxing method and their photocatalytic properties. Ceram. Int. 40, 15051–15055.
Subapriya, R., Nagini, S., 2005. Medicinal properties of neem leaves: a review. Curr. Med. Chem. AntiCancer Agents 5, 146–156.
Sundaram, R., Nagaraja, K.S., 2004. Electrical and humidity sensing properties of lead(II) tungstate–tungsten(VI) oxide and zinc(II) tungstate–tungsten(VI) oxide composites. Mater. Res. Bull. 39, 581–590.
Uko, O.J., Kamalu, N.T., 2001. The neem tree-uses and potentials. Nig. J. Exptal. Appl. Biol. 2, 223–229.
Valdez, J., Gomez, I., 2016. One-step green synthesis of metallic nanoparticles using sodium alginate. J. Nanomater. 1, 9790345–9790411.
Vignesh, K., Suganthi, A., Rajarajan, M., Sara, S.A., 2012. Photocatalytic activity of AgI sensitized ZnO nanoparticles under visible light irradiation. Powder Technol. 224, 331–337.
Vinoth, B., Manivasagaperumal, R., Rajaravindran, M., 2012. Phytochemical analysis and antibacterial activity of Azadirachta indica A. Juss. Int. J. Res. Plant Sci. 2, 50–55.
Zhang, H., Li, J.G., Zhang, H.B., Liang, X.S., Yin, C.G., Diao, Q., Zhang, J., Lu, G.Y., 2013. NASICON-based potentiometric Cl_2 sensor combining NASICON with Cr_2O_3 sensing electrode. Sens. Actuat. B Chem. 180, 66–70.